Ultra-fast bright field and fluorescence imaging of the dynamics of micrometer-sized objects

Xucai Chen,[1] Jianjun Wang,[1] Michel Versluis,[2] Nico de Jong,[3] and Flordeliza S. Villanueva[1,a)]

[1]*Center for Ultrasound Molecular Imaging and Therapeutics, University of Pittsburgh Medical Center, Pittsburgh, Pennsylvania 15213, USA*
[2]*Physics of Fluids Group, University of Twente, Enschede 7500 AE, The Netherlands*
[3]*Biomedical Engineering, Erasmus MC, Rotterdam 3000 CA, The Netherlands*

(Received 15 November 2012; accepted 20 May 2013; published online 11 June 2013)

High speed imaging has application in a wide area of industry and scientific research. In medical research, high speed imaging has the potential to reveal insight into mechanisms of action of various therapeutic interventions. Examples include ultrasound assisted thrombolysis, drug delivery, and gene therapy. Visual observation of the ultrasound, microbubble, and biological cell interaction may help the understanding of the dynamic behavior of microbubbles and may eventually lead to better design of such delivery systems. We present the development of a high speed bright field and fluorescence imaging system that incorporates external mechanical waves such as ultrasound. Through collaborative design and contract manufacturing, a high speed imaging system has been successfully developed at the University of Pittsburgh Medical Center. We named the system "UPMC Cam," to refer to the integrated imaging system that includes the multi-frame camera and its unique software control, the customized modular microscope, the customized laser delivery system, its auxiliary ultrasound generator, and the combined ultrasound and optical imaging chamber for *in vitro* and *in vivo* observations. This system is capable of imaging microscopic bright field and fluorescence movies at 25×10^6 frames per second for 128 frames, with a frame size of 920×616 pixels. Example images of microbubble under ultrasound are shown to demonstrate the potential application of the system. © *2013 AIP Publishing LLC*. [http://dx.doi.org/10.1063/1.4809168]

I. INTRODUCTION

High speed imaging has application in a wide area of industry and scientific research. It allows fast dynamic phenomena to be visualized. In medical research, high speed imaging has the potential to reveal insight into mechanisms of action of events occurring in ultra-fast time scales. Examples of this kind of study include the dynamic behavior of microbubbles (MB) at ultrasound (US) frequencies, such as contrast enhanced US imaging, US assisted thrombolysis, drug delivery, and gene therapy, as the US frequency in such applications induces events at microsecond to nanosecond time scale.[1–6]

MB used in medical applications refers to gas-filled particles that range from submicrometer to 10 μm in diameter. They typically have a shell membrane composed of albumin, galactose, lipid, or polymers. The active part of the MB is the gas core that increases ultrasound contrast relative to blood and soft tissue due to its high compressibility relative to surrounding material such as blood. Gas cores can be air, nitrogen, or perfluorocarbon (PFC). Contrast enhanced US imaging has been used successfully for organ edge delineation and blood perfusion imaging.[7] The capability of attaching targeting ligands to the surface of MB that bind to receptors characteristic of vascular diseases such as inflammation allows molecular imaging with US.[8] The capability of attaching therapeutic loads such as drug or DNA/RNA to the surface of MB for local delivery allows US-mediated microbubble destruction as a means to deliver therapeutic drugs or genes in to treat diseases such as cancer, diabetes, and limb ischemia.[9] The acoustic radiation force on the MB has been proposed to deliver biological agents such as stem cells for vascular therapy.[10] The ability of US in the presence of MB to accelerate thrombolysis shows the potential for US therapy for myocardial infarction, stroke, and microvascular repair.[11,12] The induction of nonlinear oscillation of MB under US excitation at various conditions is the basis for all contrast enhanced US imaging and therapeutic modalities. The clinical translation of such modalities, particularly US-MB therapeutics, is limited by a poor understanding of the mechanisms by which US-MB interactions exert bioeffects, which in turn is caused by an incomplete understanding of the range of MB acoustic behaviors under the influence of US. For example, little is currently known about how ultrasound-induced destruction of MBs carrying genes enhances gene transfer and expression; hence, manipulating acoustic parameters to achieve optimal results is driven not by an understanding of principles but by a trial and error approach. Thus, visualizing the unique MB acoustic behaviors that engender biological effects will be critical to developing mechanistic principles and thus to clinically optimizing therapeutic strategies that utilize MBs and US. The visual observation of the US, MB, and biological cell/tissue interactions will also help to understand the dynamic behavior of MBs *in vivo* and eventually lead to better design of molecular imaging techniques.

a)Author to whom correspondence should be addressed. Electronic mail: villanuevafs@upmc.edu.

 © 2013 AIP Publishing LLC

High speed camera systems typically have two configurations, one using a single sensor and fast switching, the other using multiple sensors. Commercially available high speed cameras use a combination of mechanical and electronic shutters to control the exposure time in conjunction with a charge coupled device (CCD) or complementary metal-oxide-semiconductor (CMOS) based photo-sensor chip. One such system is capable of acquiring 16 000 frames per second (fps) at full HDTV resolution of 1280 × 800 pixels, with a pixel size of 28 × 28 μm (Phantom v1610, Vision Research, Wayne, NJ). This camera is also able to acquire images at 1 Mfps, but at reduced resolution of 128 × 16 pixels. An imaging sensor using the *in situ* storage image sensor (ISIS) technology that can capture 100 consecutive frames at 1 Mfps with 312 × 260 pixels has been reported.[13] Memory elements were attached to every pixel and image signals were stored in the *in situ* storage without being read out of the sensor. However, the fill factor was only 13%, and the effective pixel size, too large at 66.3 × 66.3 μm, was not suitable for microscopic observations (pixels too large for required spatial resolution). Newer design with the ISIS technology incorporates charge-carrier multiplication (CCM), a signal amplification device. High sensitivity is achieved when cooling is also used. The latest version of the device can capture 117 frames at 16 Mfps with 262 × 456 pixels.[14] Still, the effective pixel size of 43.2 × 43.2 μm makes it undesirable for microscope application (pixels still too large for the required spatial resolution).

By using multiple sensors, framing cameras can reach maximum frame rates up to 200 Mfps. Typically, a framing camera splits the incoming image into several optical channels with beam splitters, dichroic mirrors, prisms, or a pyramid, with an image sensor mounted in each channel. High frame rates are made possible by further using special shutters. One such camera uses the fast switching capability of gated image intensifiers to reach a frame rate of 200 Mfps (Imacon 468, DRS Technologies, Tring, UK). However, the record length, equivalent to the number of frames, is limited by the number of independent optical channels available. In addition to the cumulative cost of multiple channels, the number of optical channels is also limited by the photons available for each image, as each splitting divides the image intensity.

Higher number of frames can be achieved in rotating mirror based cameras. A fast rotating mirror is used to sweep the image along a photographic film or an array of CCDs mounted on an arc. The first rotating mirror film camera was used to image the first hydrogen bomb explosion test in 1952.[15] Special mechanical shuttering was necessary to prevent multiple exposures. Frame rates of 25 Mfps were achieved, with a record length of 130 frames.

To address imaging that demands high frame rates, high frame numbers, high sensitivity, and high resolution, a high speed rotating mirror system using CCDs was custom built for medical research investigations on MB behaviors in US fields.[16] The system, dubbed "Brandaris," uses 128 high sensitivity CCDs (ICX055AL, Sony Corp, Tokyo, Japan) and is capable of acquiring a maximum of 128 frames at up to 25 Mpfs. The CCD chip has 500 × 582 photosensitive cells, with a cell size of 9.8 × 6.3 μm. Since there was one transport channel per two photosensitive cells (interlaced sampling), the effective pixel count per image was 500 × 291, and an effective pixel size was 9.8 × 12.6 μm. This system, which is not available commercially, has been extensively used to make *in vitro* observations of MB dynamics in US fields that have suggested that MB acoustic behaviors may have unique therapeutic and diagnostic utility in medicine.[17–24]

Until recently, multi-frame high-speed cameras at million frames per second rate were capable of bright field imaging only. US-induced MB oscillations *in vivo* have not been visualized at Mfps rate, mainly due to low optical contrast of MBs relative to tissue and blood background. Therefore, it has not been possible to evaluate US-induced MB behaviors *in vivo* under the influence of surrounding tissue, flow, and other blood cell components. *In vivo* imaging of MB requires fluorescence labeling of MBs to distinguish them as distinct from blood cells and surrounding tissue. Multi-frame microscopic fluorescence imaging of MBs at nanosecond exposure times has been a challenge to achieve. A recent update of the Brandaris system reported on the improvement on fluorescence imaging at above 1 Mfps rate, among other improvements such as region of interest selection mode and segment selection mode.[25]

We present the development of a high speed bright field and fluorescence imaging system that further improves on the sensitivity, spatial resolution, and computer control, that synchronizes light source for bright field and laser fluorescence imaging, and that incorporates external waves such as US. Special emphasis is put on *in vitro* and *in vivo* fluorescence imaging where photon availability is limited and high sensitivity is required. The proposed system is ideally suited to US-MB investigations, which typically exhibit dynamics of interest in the nanosecond regime. At a spatial resolution of 0.5 μm and temporal resolution of 40 ns, MB surface velocities on the order of 12.5 m/s can be recorded, sufficient to document the violent collapse of MB during initial cavitation that might be responsible for many of the relevant bioeffects of interest to clinical translation of US-MB technologies. The record length of 128 frames, corresponding to 5.12 μs at 25 Mfps, is sufficient for the study of MB dynamics at relevant frequencies for US imaging (higher than 1 MHz) as a typical imaging pulse is less than 4 acoustic cycles.

II. SYSTEM DESCRIPTION

A. System overview

Through collaborative design and contract manufacturing, a high speed imaging system has been successfully built at the University of Pittsburgh Medical Center (now marketed as Model 510, Cordin Company, Salt Lake City, UT). We have named the system "UPMC Cam," to refer to the integrated imaging system that includes the multi-frame camera and its unique software control, the customized modular microscope, the customized laser delivery system, its auxiliary US generator, and the combined US and optical imaging chamber for *in vitro* and *in vivo* observations of US-induced events. A simplified schematic diagram of the UPMC Cam is illustrated in Fig. 1. The subsystems enclosed in the dashed outline in Fig. 1

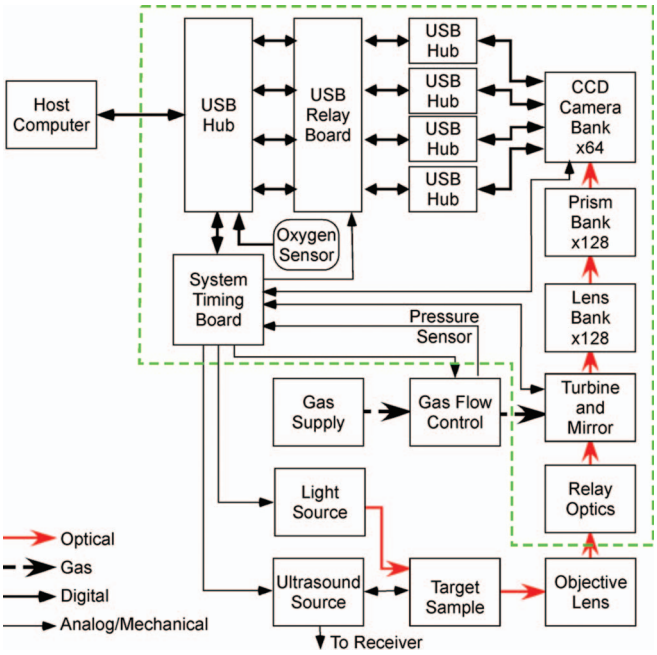

FIG. 1. Schematic diagram of the imaging system. Minor subsystems such as oxygen sensor, pressure monitor, and temperature were omitted from the diagram.

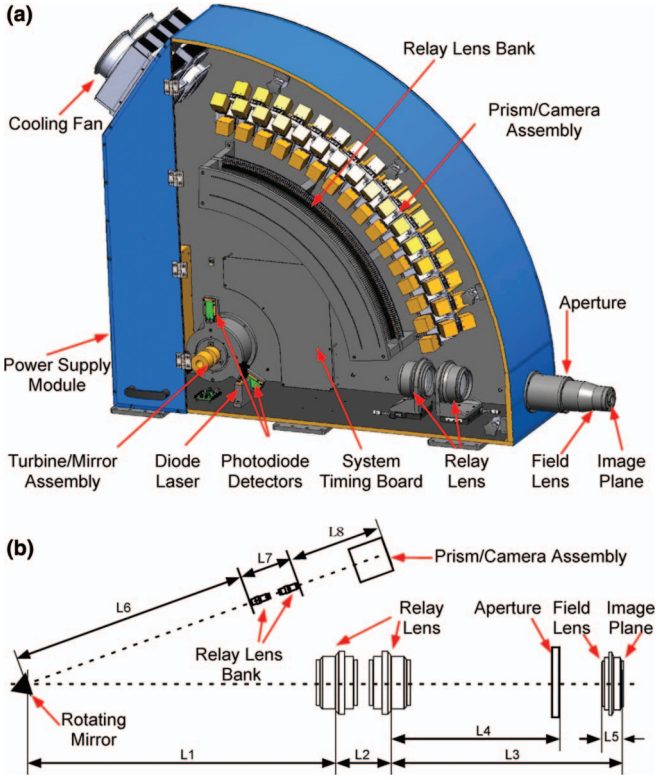

FIG. 2. (a) A drawing of the main camera system. For clarity, all USB hubs and relay circuits were removed from this drawing. (b) Overall optical design. $L_1 = 720$ mm, $L_2 = 130$ mm, $L_3 = 527$ mm, $L_4 = 383$ mm, $L_5 = 18$ mm, $L_6 = 563$ mm, $L_7 = 78$ mm, $L_8 = 260$ mm. Distances listed are approximate and adjustable. With these parameters, the camera system has a demagnification factor of 0.62. Detail for prism/camera assembly is shown in Fig. 3.

are housed within the Cordin 510 enclosure, shown in a drawing in Fig. 2(a).

The camera system is based on the rotating mirror framing camera. An external image, either from a microscope or another source, is projected onto the rotating mirror prism. The mirror prism is rotated by a gas turbine at high speed, up to 20 000 rotations per second (rps), and directs the incoming image through a bank of lens pairs to a bank of CCD cameras. In-between the lens bank and the CCD cameras, a bank of specially oriented mirror prisms is used to project two 2 image frames onto each CCD camera. The prism/camera assemblies are arranged in an arc such that 128 temporally separated images are spatially projected on to 64 CCDs. This optical arrangement is developed in order to realize a higher total number of frames using the limited space in a small housing system.

The gas turbine is operated with a gas flow controller (500 series, Cordin Company, Salt Lake City, UT). For each rotation of the rotating mirror, a master synchronization signal is generated by using a laser diode and a pair of photodiode detectors. This signal is used to provide real-time feedback of turbine speed for control and display.

The system timing board is the central control for the system. It provides trigger logic to all CCD devices, provides the electrical interface to the user I/O panel, provides the interface to the turbine flow control system, and is used as an interface to the oxygen sensor (to measure displacement of oxygen by helium for high speed mirror operation). The trigger logic relies on synchronization of all cameras to rotating mirror angle detection events. Timing parameters for the capture of an image sequence are set from the host computer via the user interface on the host computer. This allows setup of desired recording period, external laser timing, and US trigger timing. These timing parameters are sent via a USB link to the system timing board. The trigger for the cameras is directed from the system timing board to a trigger buffer board, which provides a simultaneous trigger signal to all 64 CCD cameras.

A strobe light (MVS-700, PerkinElmer, Salem, MA) triggered from the system timing board serves as the light source for bright field imaging. A custom fast pulse capable Cyan-488 optically pumped semiconductor (OPS) laser system (Genesis MX488-5000, Coherent, Santa Clara, CA), also triggered from the system timing board, is used for fluorescence imaging. A custom fiber optics alignment system is used to deliver the laser power through the microscope.

The system timing board also provides a trigger signal for US generation for studies where US-induced high speed events are being observed. For a typical application, an arbitrary function generator and a gated radio frequency power amplifier are used to drive the US transducer.

The system is capable of imaging bright field and fluorescence movies at 25 Mfps for 128 frames, with a frame size of 920×616 pixels. For *in vitro* and *in vivo* studies of biological cells, MBs, or small blood vessels during exposure to US, the camera is directly coupled to the output of the microscope. For other applications, the coupling can be removed to accommodate other objective lens such as telephoto- or macro-lenses.

B. Optical design

The overall optical design used for the current system is provided by Parker.[26] As with the Brandaris camera, the optical design is based on the Miller principle. An image is formed by a camera's objective and relay lens on or near the face of the rotating mirror. As the mirror rotates, the image is swept across an arc of relay lenses that sequentially relay the images at the face of the mirror to the bank of CCDs positioned in an arc shaped track. The optical property known as the Miller principle, named after its discoverer, David Miller,[27] states that the images will be nearly stationary when recorded in each frame of the camera if the image is formed at the proper position near the surface of the rotating mirror. Ideally, the image should be on the rotational axis of the mirror. However, as the mirror must have a finite thickness, the exact location is found by adjusting the relay lens location such that minimal residual image drag (an image artifact caused by the finite mirror thickness and imperfect positioning) on the CCD bank is achieved. A detailed analysis of the optical requirement is provided by Igel and Kristiansen.[28]

The overall optical path of the system is shown in Fig. 2(b). An external image, from a microscope or another source, is positioned on the first image plane. A pair of 610 mm NIKKOR lenses (Nikon Inc., Melville, NY), mounted on micrometer driven translation stages, is used to relay the first image plane to a three-sided rotating mirror. For our application, only one of the three mirror surfaces is reflective. The image entrance stop, a rectangular shaped slit aperture (2.2 × 43.5 mm), is used to reduce image drag by shaping the optical beam of the image. The aperture is designed such that its image is the same shape and size as the framing lenses in the lens bank. The image on the rotating mirror is then reflected through 128 sets of relay lenses, each set for each of the images, to the 64 CCDs arranged in an arc around the rotating mirror. The relay lenses are arranged with an angular spacing of 0.576° so the effective frame rate F_r (in fps) is related to the turbine speed R (in rps) by $F_r = 1250\,R$.

Due to limited space of the overall camera housing, only 16 frames would have been realized if the CCDs were installed in a linear fashion along the image arc. It is fortuitous that the relatively large format of the chosen CCD allows the storage of 2 consecutive images. The dual imaging of 2 frames onto a single CCD is accomplished by using pairs of mirrors to direct each image to one section of the corresponding CCD (Fig. 3). To increase the number of frames further, banks of four CCDs are arranged in a three-dimensional fashion, with each CCD in the bank following a different optical path by using mirror prisms at different angles. CCDs are positioned at 90° (frames 1 and 2), −45° (frames 3 and 4), 45° (frames 5 and 6), and 90° (frames 7 and 8) with respect to the main optical axis. Overall, 16 such banks of CCDs are used, totaling 64 CCD cameras, capable of 128 frames per requisition. Focus and alignment are precisely controlled through a series of positioning systems. The image magnification is adjusted by changing the distance between the pairs of relay lenses. Focus is adjusted by changing the relative position of the relay lenses with respect to the CCD. The X and Y positions of the image on the CCD are adjusted by the turning mirrors in the CCD bank, and the angular position of the image on the CCD is adjusted by a rotary table mounted to each CCD.

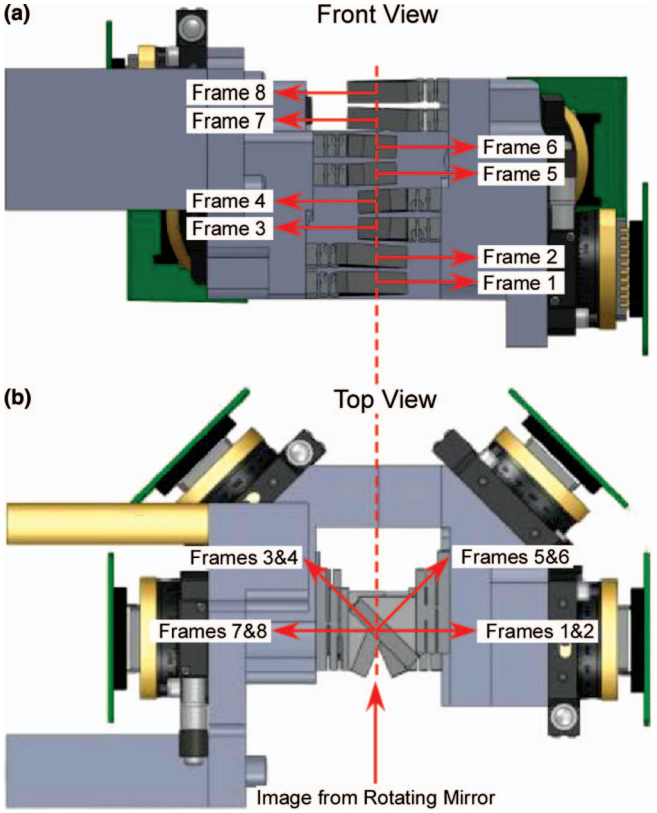

FIG. 3. Camera optics. CCDs were arranged in banks of 4, with each CCD in the bank following a different optical path. (a) Front view as observed from the travel path of the image. (b) Top view showing the different light paths for each image. In this drawing, the outer casings of the cameras were removed to reveal the board level CCDs.

With the dimensions shown in Fig. 2, the camera system has a demagnification factor of 0.62. With a 100× objective lens, the overall optical magnification of the system is 62×. With the chosen CCD pixel size of 6.45 μm and image size of 920 × 616 pixels, the image on the CCD is 5.93 × 3.97 mm, corresponding to a field of view of 96 × 64 μm. This field size is sufficient for single MB studies as well as multiple MB studies where secondary radiation force is important. This size is also appropriate for *in vivo* studies in the microcirculation where MB-vessel wall interaction is important.

C. Turbine control

The gas turbine used is a Model 1220 Gas Driven Rotating Mirror assembly (Cordin Company, Salt Lake City, UT), designed to use air, nitrogen, or helium as the pressure source. The gas turbine can be operated under two different configurations depending on the desired top rotating speed. The Model 500 series gas control box (Cordin Company) operates the turbine up to 4000 rps (corresponding to 5 Mfps) with a 690 kPa air or nitrogen supply and 20 000 rps (corresponding to 25 Mfps) with a 760 kPa helium supply.

An infrared laser diode, internally mounted off the optical axis, is directed at the rotating mirror to provide timing information. Two photodiode detector circuits, one mounted

a few degrees before and the other mounted a few degrees after the set of relay lens banks in the arc of rotation, are used to pick up the timing signals which, for each rotation of the rotating mirror, form the rising and trailing edges of a master synchronization signal and provide real-time feedback of turbine speed for control and display. This configuration is distinct from that in the Brandaris, where only one photodiode detector is used. The dual photodiode detector design allows the turbine speed to be measured in 1/5 of a rotation of the mirror. Each photodiode detector also provides a redundant measurement of the turbine speed every mirror cycle. This dual detector design in conjunction with the system timing board allows advanced timing control of the imaging system.

The system control board provides a continuous update of mirror turbine speed. This speed value is communicated continuously to the host computer for display. The turbine speed value is also used by the system timing board for turbine speed control. The microcontroller on the turbine speed control uses a proportional–integral–derivative (PID) controller algorithm. This uses the target-speed variable from the host and the speed variable (or pressure variable) from the field-programmable gate array (FPGA) on the system control board to provide an analog control to the turbine proportional control valve. The PID controller forces the turbine speed value to equal the target speed set point. During default operation, the system control board is armed to initiate a sequence of events (see Sec. II I) once the turbine reaches a range, typically 1%–2% of the target rate, set by the operator. The exact turbine speed at the moment of image acquisition is recorded to indicate the true frame rate.

D. CCD

Our system contains 64 pre-fabricated Lm165M (Lumenera, Ontario, Canada) digital cameras that utilize the ICX285AL CCD chip (Sony Corp, New York, NY). The ICX285AL is an interline CCD solid-state image sensor with an array of square pixels. It has 1360 × 1024 effective pixels of 6.45 × 6.45 μm size. High sensitivity and low smear are achieved through EXview HAD CCD technology. Progressive scan allows signals from all pixels to be output independently within approximately 1/15 s. The electronic shutter with variable charge-storage time allows full-frame still images without a mechanical shutter.

The Lm165M is designed for a variety of industrial and scientific applications, particularly those with low-light conditions where high dynamic range is required. It uses a locking industrial mini USB 2.0 digital interface and RJ45 GPI/O connector for peripheral control and synchronization. It has a bit depth of 12 bits; either 8 bit or 12-bit data can be selected. On-board memory of 32 MB is available for frame buffering. The high sensitivity, high resolution, high dynamic range, and the compact body (measuring 44 × 44 × 56 mm in size) of the Lm165M made this system a top choice for our application among other candidate cameras considered. Custom firmware upgrade was provided by the manufacturer during the development of our project.

E. System timing board and USB relay

The system timing board provides trigger logic to all CCD devices, the electrical interface to the user I/O panel, and the interface to the turbine flow control system. It is used as an interface to the oxygen sensor that measures the displacement of oxygen (and by that nitrogen) by helium within the camera enclosure for high speed mirror operation. The trigger logic relies on synchronization of all cameras to rotating mirror angle detection events as measured by the photodiode detectors. Timing parameters for the capture of an image sequence are set from the host computer via the user interface on the host PC to the system timing board. This allows setup of the desired recording period, external light source timing, and US trigger timing. The trigger for the cameras is directed from the system timing board to a trigger buffer board, which provides a simultaneous trigger signal to all 64 Lm165M cameras. TTL-level trigger signals to external devices such as light sources and US generators are provided from the timing board with a rear mounted control panel. The master synchronization signal from the turbine/mirror assembly and the CCD integration control signals are also made available on this panel for diagnostic purposes.

An additional function of the system timing board is to provide a delayed activation of individual Lm165M cameras. Upon system startup, all Lm165M cameras are isolated from the host computer (see Fig. 1). The host software activates a group of 16 cameras at a time, allowing about 5 s of time for each of the 16 cameras to be enumerated by the host computer, before activating the next group. This design is necessary to avoid a conflict with the host system when a large number of USB devices are activated simultaneously.

The Lm165 m has a delay of approximately 47 μs after it receives a trigger signal before integration starts.

F. Custom microscope and camera mount

A custom optical table (PTM11109/LS-S12, Thorlabs Inc., Newton, NJ) is used to support the camera system and the microscope to reduce the effect of room vibration, as shown in Fig. 4. The microscope is mounted on an extension table off the optical table with an x-y translation stage to allow alignment of the image from the microscope to the camera optics in the horizontal directions. Additional alignment in the vertical dimension is accommodated with the upper focusing block on the microscope.

A modular upright microscope (BXFM, Olympus Corp, Tokyo, Japan) was custom designed with a flexible focus mount. The BX-RFA-KAI illuminator has dual side ports to allow a laser light source. A dual focusing block arrangement allows focusing on the sample while keeping the optical alignment with the camera. Sample handling is accomplished with a motorized platform stage (MP78-Z-BX-FM, Olympus) and focusing of the sample is achieved with the lower focusing block, with custom adaptors between the focusing block and the objective lens. Motions in all three directions are controlled remotely with a motorized micromanipulator (MP-285, Sutter Instrument Company, Novato, CA). To assist in fast switching of image magnification, a

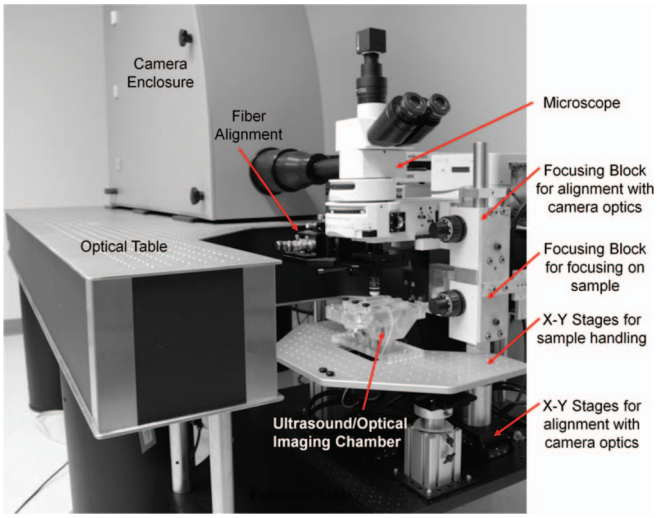

FIG. 4. Microscope coupling to camera system. The camera is mounted on a custom optical table. The microscope is mounted on an extension table off the optical table with an x-y translation stage to allow alignment of the image from the microscope to the camera optics. Additional alignment in the vertical dimension is accommodated with a second focusing block on the microscope.

magnification changer is included (U-CA, Olympus) with 1×, 1.25×, 1.60×, and 2× further enlargement. The image is diverted to the rotating mirror system with a dual port intermediate unit (U-DP, Olympus). This unit can serve a variety of purposes such as image separation by spectral composition, input for an additional illumination source, or output of an image. It is used as an image output with an image formation lens (U-DP1xC, Olympus) for normal operation in our system. An additional camera port is mounted on top of the microscope with a camera adaptor (U-TV1x-2, Olympus) for remote focusing adjustment, normal frame rate observation, and recording.

For applications where US is used to manipulate the sample, high numerical aperture water immersion objective lenses are used. The 60× lens (LUMPLFLN 60X/W, Olympus) has a numerical aperture of 1.0 with a working distance of 2.0 mm; the 100× lens (LUMPLFL 100XW/I, Olympus) has a numerical aperture 1.0 and a working distance of 1.5 mm.

G. Laser illumination

A custom fast pulse capable Cyan-488 OPS laser system (Genesis MX488-5000, Coherent, Santa Clara, CA) is used for fluorescence imaging. The laser is driven with a pulsed current power supply (AV-106B-B, Avtech Electrosystems, Ogdensbugh, NY), triggered from the system timing board. The laser system has a wavelength of 488 nm and is rated at 5 W. It can be operated at a pulse repletion frequency (PRF) of 100 Hz with a 20-μs pulse duration and a PRF of 10 Hz at 200-μs pulse duration, with much shorter pulse durations available. The rise time of the laser pulse is less than 1 μs. During image acquisition, the laser source is triggered from the camera system such that a single laser pulse covers all 128 frames, starting 2 μs before the first frame and ending 2 μs after the last frame. This design allows relatively low total light exposure to the sample (about 45 μJ for 25 Mfps at maximum power setting) and reduces photobleaching to the sample. Laser energy used per frame is 200 nJ at 25 Mfps. In the updated Brandaris, a continuous wave laser was used in conjunction with an acousto-optic modulator as a gate.[25]

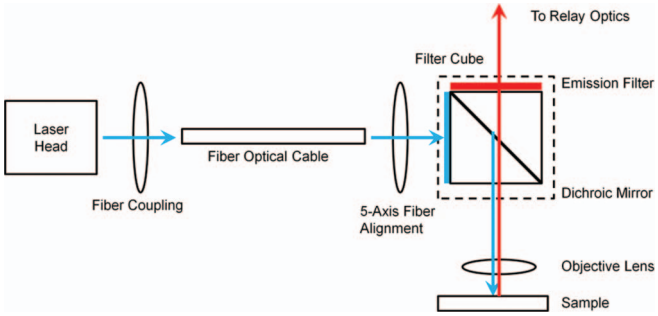

FIG. 5. Laser alignment and imaging light path. A 5-axis fiber alignment system (3 for x-y-z position adjustment and 2 for tilt angle adjustment–details not shown) is used to optimize the delivery efficiency through the microscope and adjust the spot size of the laser on the sample.

The full optical path for laser fluorescence is shown in Fig. 5. The pulsed laser light energy is collected with a weakly focusing lens and is transmitted through an optical fiber. A 5-axis positioning system is used to align the laser light to the objective lens of the microscope (details not shown). A 16-mm C-mount lens collimates the light out of the optical fiber and directs it toward the specially configured filter cube. The distance between the end of the optical fiber and the 16-mm lens is used to adjust the laser spot size on the sample to be imaged. The illumination onto the sample can be approximated as a homogenized Gaussian beam. For components used for our construction, the laser spot size can be adjusted in the range of 25–130 μm with a 60× water immersion objective lens and 20–70 μm with a 100× water immersion lens. This design allows the illumination intensity to be increased while sacrificing the field size in extremely difficult conditions where tissue attenuation causes light energy loss and or lower fluorophore label could not be increased. In some applications, it is necessary to illuminate a big enough size (for example, a bed of microcirculation in a small animal) to study the effect of local environment such as the presence of red blood cells on the MB behavior. In other applications, higher intensity light is needed to shine on a single MB to cause photoacoustic phenomena or droplet vaporization for the study phase transition to create MB as an ultrasound contrast agent.

A special filter cube is mounted on a side facing position. The excitation filter is not used for this application but a short-pass filter could be used to remove any infrared radiation. The dichroic mirror (Di01-R488-25 × 36, Semrock Inc., Rochester, NY) is chosen to reflect effectively at the laser wavelength (>98%) but passes at longer wavelength (transmission > 93% for 503.3-900 nm). The emission filter (BLP01-488R-25, Semrock Inc., Rochester, NY) is a long-pass filter to allow maximum detection of fluorescence signal (average transmission > 93% for 504.7-900 nm).

H. Imaging chamber, sample handling, and US system

A custom built imaging chamber (Fig. 4) was fabricated to allow simultaneous optical observation and US delivery and detection. The target to be studied is positioned in the co-focal area of light (the optical field of view) and US beams. The chamber is filled with de-gassed de-ionized water, de-gassed filtered saline solution, or other suitable medium for optical and US transmission. For *in vitro* observation, a hollow cellulose fiber of 200 μm inner diameter to hold the sample is mounted on two hypodermic needles with Luer lock connectors. For *in vivo* studies, the sample holder is replaced with a small animal stage.

The external US source is generated with an arbitrary function generator, triggered from the camera system, a radio-frequency (RF) power amplifier, and a US transducer. In some applications, a second US transducer is used to perform passive or active cavitation detection. The co-localization of optics and ultrasound is achieved by using false objectives. The false objective is an object that has the same mounting as the regular objective lens, with a needle tip located at the focal plane of the regular objective. Standard pulse-echo method is used to localize the needle tip in the focal area of the US transducer by moving the imaging chamber with a motorized 3D translation stage. Typically, the US beam size is much larger (on the order of mm) than the laser illumination size and the optical field of view.

I. Firmware and software control

The firmware uses the master synchronization signal to set and control the key image capture timing parameters. The master synchronization pulse is used to generate signals that define the start and end of the CCD exposure interval (Fig. 6). The time between successive sync pulses is used to determine the turbine rotation speed. The time between the rising edge and falling edge of a synchronization pulse is measured by the timing board to produce a redundant turbine speed estimate for advanced timing control. Camera integration time control is derived from these sync signals. The timeline starts with a trigger pulse (logically derived or manual). Following the trigger pulse, the timeline logic waits for the next sync pulse rising edge. The rising edge of the first sync pulse following the trigger is used as the time base (the time-zero event). All capture timing logic starts at the time base, calculated with the measured turbine rotation speed at that time.

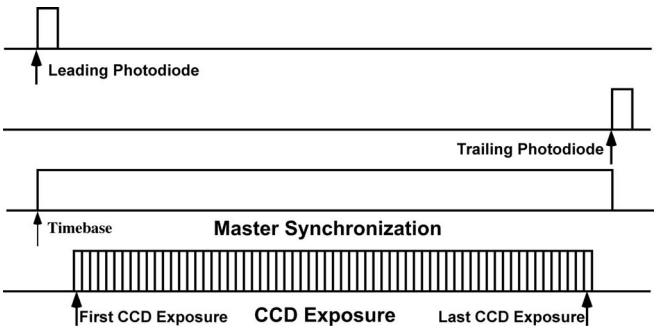

FIG. 6. Abbreviated timing diagram for image capture. The dual photodiode detector circuits provide redundant measurement of the speed and location of the rotating mirror.

The host software runs on a Dell Precision T-5500 quad-core workstation with Intel Xeon Processor, with 16 GB of memory (Dell Inc., Round Rock, TX) and Windows 7 operating system (64-bit version, Microsoft Corp., Redmond, WA). The host computer communicates with the camera system via a single USB interface cable. Upon initial startup, the host checks the integrity of the system timing board, and enumerates the individual Lm165M cameras in a delayed fashion via the relay board. The host software then checks for the gas pressure and helium level in the camera chamber. A default image capture sequence is summarized as the following: (1) the camera capture interval (integration time), gain, and choice of binning are defined on the host software and sent via USB link to each Lm165M camera; (2) the system timing board is put into an armed state with a command from the host software and sent via the USB interface from the host computer; (3) the system timing board receives a trigger, initiated from the host software when a desired speed set-point is reached or by manually triggering from the host software; (4) the system timing board awaits the next sync signal, and calculates the required timing values for the CCD, the light source (laser or strobe light), and US triggers from the sync signal, based on mirror rotation speed (inherent delays in the camera trigger and travel time for US are taken into account); (5) trigger signals for external devices such as light source and US source, if enabled, are generated by the system timing board and sent via the User I/O panel off the timing board; (6) a trigger signal is generated (before or after the trigger signals for external devices) and distributed to the CCDs through the trigger buffer board from the system timing board, timed such that the CCDs receive the signal 47 μs (the camera delay) before the next sync pulse; (7) CCD integration starts when the camera delay interval finishes and continues during the pre-programmed capture interval on all cameras simultaneously; (8) when the capture interval is complete, charge transfer from the photo-sensors on the CCD to the transfer registers occurs (less than 1 μs), after which image transfer to the frame buffer starts (lasting less than 65 ms); (9) if selected, a second movie is captured during image transfer, with the image held in the photodiode array until the first image in the shift registers has been transferred to the first frame buffer (triggers for the light sources and ultrasound source may also be selectively programmed for the second movie); and (10) the second image is transferred to the second frame buffer.

Our camera system can handle advanced trigger for external devices such as US generation, up to 510 mirror cycles. For 5 Mfps, this means we can trigger the US accurately up to 125 ms ahead of image acquisition. Even at 25 Mfps, we can trigger accurately 25 ms ahead of image capture.

J. Other components

1. Power supply

The power supply unit used for the 510 camera (components within the dashed outline in Fig. 1) is EM shielded from the camera electronics. The overall current drawn of the

camera system (excluding host computer, light source, and US source) with all Lm165M powered up is about 545 W.

2. Cooling

The camera chamber is cooled to maintain the temperature below 25 °C for normal ambient temperature. Cooling is achieved with two thermoelectric coolers mounted near the top of the cabinet.

3. Camera enclosure

The enclosure is made of 12.7 mm thick aluminum plates. All panel connections have O-rings installed to reduce the amount of helium loss.

K. Photon analysis for high speed microscopic fluorescence imaging of MB

The design of our system for high speed microscopic fluorescence imaging required consideration of multiple factors, including the choice of CCDs (sensitivity and spatial resolution), illumination (the light source and effective delivery), the fluorescence labeling of the MB, and the microscope (photon collection efficiency). For fluorescence imaging of the MB with the laser system described earlier, the input photon flux on sample can be described as $I_{in} = W/(A_I e)$, where W is the total laser power delivered to the sample, A_I is the area of the illumination, and $e = hc/\lambda$ is the energy per photon, $\sim 4 \times 10^{-19}$ J/photon at 488 nm. The output photon flux from one MB can be expressed as $P_{out} = I_{in} n \sigma_t Q_e$, where n is the number of dye molecules per MB, σ_t is the extinction cross section per dye molecule, and Q_e is the quantum efficiency of the dye. The area of the MB image on the CCD is $A_C = A_B X^2$, where A_B is the geometric cross section of the MB and X is the overall magnification of the whole system. Therefore, the average photon flux on the CCD in the MB image is $I_{out} = Q_0 P_{out}/(A_B X^2)$, where Q_0 is the overall photon collection efficiency of the total optical system, including the objective lens, the dichroic mirror, the emission filter, and the optical relay system in the rotating mirror camera. The value of Q_0 is about 0.2, largely limited by the numerical aperture of the objective lens. The number of photons per pixel per frame is $S_{out} = I_{out} t_E A_P$, where t_E is the effective exposure time and A_P is the area of the square pixel on the CCD. The effective exposure time of the rotating mirror system is one half of the inter-frame time,[24] which in turn is equal to the inverse of the frame rate. Combining the above relationships, we have the number of photons per pixel per frame as

$$S_{out} = (W/e)(n\sigma_t/A_B) Q_e Q_0 . t_E (A_p/A_I)/X^2. \quad (1)$$

The quantity $(n\sigma_t/A_B)Q_e$ is simply the total emission cross section of the dye on the MB normalized by its geometrical cross section. Normally, the value of this quantity is much smaller than unity. Otherwise, substantial self-quenching would occur. It should be noted that Eq. (1) should be considered a rough estimate only. In practice, the fluorescence image of MB is defined by the equator only, where the photon density is substantially higher than the average photon density in the MB image. Also, only half of the dye molecular facing the objective lens is available for image formation. The effect of relaxation time of the dye molecular is not considered either but may play a major role in the quantitative analysis as exposure time is of the same order of amplitude as the relaxation time.

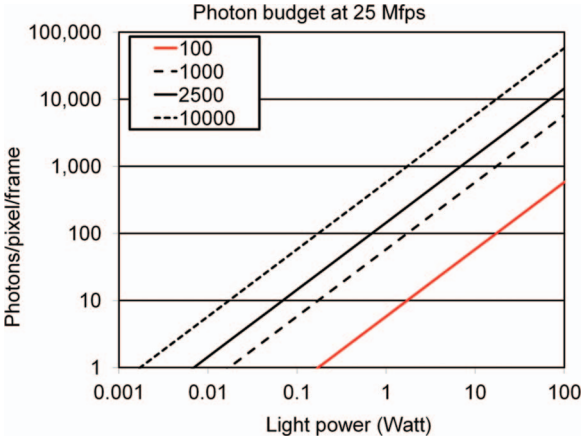

FIG. 7. Estimated number of photons available for image formation in high speed fluorescence mode, for several surface density of the dye (100, 1000, 2500, and 10 000 molecules/μm^2). For this calculation, the fluorophore is R-PE, with extinction cross section of 3.26×10^{-15} cm^2 and quantum efficiency of 0.82. Other parameters used: pixel size 6.45 μm, illumination size 50 μm, $X = 62$, $Q_0 = 0.20$, $t_E = 20$ ns.

Equation (1) provides guidance for improving the image quality. For example, for a fixed light source at a fixed frame rate, increasing the relative total emission cross section of the dye by either increasing the surface density of the dye or the emission cross section would make more photons available for imaging. On the other hand, increasing the size of the CCD pixel does not help as increased magnification is required to reach the resolution requirement. However, reducing the size of illumination can provide more photons available for imaging in some applications. Figure 7 illustrates the relationship expressed in Eq. (1) as a function of laser power for several surface densities of dye molecules.

Streptavidin coated polymeric (poly-DL-lactide, or PDLLA) MBs (CardioSphere) supplied by Point Biomedical (San Carlos, CA) were used for the initial testing of the camera system. The conjugation of biotinylated R-Phycoerythrin (R-PE) (Invitrogen, Life Technologies, Grand Island, NY) was carried out using biotin streptavidin interaction.[29] In brief, 0.2 ml of MB (5 e8/ml concentration) was mixed with 0.2 ml biotin R-PE (0.36 mg/ml) in phosphor buffered saline (PBS) for 1 h at room temperature. The mixture was washed by adding 1 ml PBS followed with centrifugation at 200 g for 3 min. The subnatant was discarded and the MBs were resuspended in 0.2 ml PBS for subsequent testing. The amount of R-PE on the surface of MB was measured using quantitative flow cytometry.[30] The intensity of the R-PE labeled MB was correlated to the number of R-PE molecules. By comparing the fluorescent intensity of the MB coated with R-PE and that of the standard microspheres (Quantum R-PE, Bangs Labs, Fishers, IN), the average number of R-PE was calculated from the linear calibration curve generated using the

standard microsphere. The density of R-PE on the MB was around 2500/μm^2, which corresponds to 70 000 molecules for a 3-μm MB. This dye density is used in Fig. 7 to estimate the number of photons available for image formation (solid black line), indicating that it is possible to form a usable image at 25 Mfps with 1-5 W of peak laser power.

III. SELECTION OF OPTIMAL CCD CAMERA

One of the most important parameters used in selecting the sensor for this system is the sensitivity, as the frame rate for fluorescence imaging has traditionally been limited by the scarcity of photons available to form an image.

Digital cameras have far surpassed film in terms of sensitivity to light, with ISO equivalent speeds of up to 204 800. The determination of ISO speeds with digital still-cameras is described in ISO 12232:2006. It gives digital still camera manufacturers a choice of five different techniques for determining the exposure index rating at each sensitivity setting provided by a particular model. The exposure index rating can depend on the sensor sensitivity, the sensor noise, and the appearance of the resulting image depending on the technique selected.

Due to spatial resolution requirements for microscopic observations, CCDs with effective pixel size larger than 20 μm were excluded from consideration. This limit allowed a 1-μm object to be imaged with at least 3 pixels in one dimension when a 100× objective is used. Some of the final candidate sensors considered are listed in Table I. All candidate CCDs have similar high quantum efficiency, better than 60% at the wavelength of interest (around 550 nm). The Sony ICX055AL was used in the Brandaris system. From the available data provided by the manufactures, the ICX429ALL and ICX285AL are 2.6× and 2.8× more sensitive compared with the ICX055AL. The direct comparison between the Sony chips and the TI EMCCD was not possible from the product specifications. However, one manufactured camera utilizing the ICX285AL, the Lumetrix 500A Imaging Photometer (MG Optical Solutions GmbH, Germany), reports the luminance sensitivity at 0.015 cd/m^2. It is equivalent to 0.18 lux, similar to the sensitivity given for the TC285SPD.

A relative sensitivity test was performed for selecting the sensor. A TV chart was used as a target. A LED was driven to provide a single light pulse at various durations. A diffuser was used to create a uniform illumination of the target. The target was imaged with all candidate cameras at several gain, contrast, and brightness controls. The image brightness was analyzed in selected regions of interest. Curves of image brightness vs. light level curves were generated (Fig. 8). The following parameters related to the sensitivity of the cameras were derived:

S_0: Slope of the image brightness vs. light duration curve in the middle of the data range, analogous to the definition used for ISO number for films, normalized by the total possible data range of the camera;
S_1: Slope of the image brightness vs. light duration curve in the middle of the data range, normalized by the total possible data range of the camera and pixel area;
L_{02}: Light level at SNR = 2 (usable image).

IV. RESULTS

A. Main characteristics

Table II lists the main characteristics of the UPMC Cam in comparison to other high speed camera types. The imaging system is capable of 25 Mfps for both bright field and fluorescence imaging, with a frame number of 128, and a frame size of 920 × 616 pixels. The system is capable of capturing a second movie, with a minimum time lag of 50 μs.

TABLE I. Comparison of sensor sensitivity.

	Brandaris	Candidate 1 Lumenera Lm165M	Candidate 2 Watec 902H	Candidate 3 Hamamatsu C9100-02
Chip set	Sony ICX 055AL	Sony ICX 285AL	Sony ICX 429ALL	TI MC285SPD-L0B0
Pixel count	500 × 582	1360 × 1024	768 × 494	1004 × 1002
Unit cell size (μm)	9.8 × 6.3	6.45 × 6.45	8.4 × 9.8	8.0 × 8.0
Effective pixel size (μm) for single shot	9.8 × 12.6	6.45 × 6.45	8.4 × 19.6	8.0 × 8.0
Scanning system	2:1 interlace	Progressive	2:1 interlace	Progressive
Analog/digital	Analog—frame grabber needed	Digital 12 bits	Analog—frame grabber needed	Digital 14 bits
Sensitivity under standard condition I[a]	500 mV typical 1/250 s	1300 mV typical 1/100 s	1400 mV typical 1/250 s	...
Saturation[a]	630 mV min.	850 mV min.	1000 mV min.	
Dark signal[a]	2 mV max	11 mV max	2 mV max	0.005 mV typ 0.02 mV max
Quantum efficiency at 550 nm (%)		>60	>60	>60
Relative normalized slope S_0[b]	1 (reference)	Various up to 27	Various up to 31	Various up to 17
Relative normalized slope S_1[b]	1 (reference)	Various up to 34	Various up to 23	Various up to 17
Relative light level at SNR = 2 L_{02}[b]		2.6		1 (reference)

[a]Manufacture provided data. Sony standard imaging condition I: Use a pattern box (luminance: 706 cd/m^2, color temperature of 3200 K halogen source) as a subject. Use a testing standard lens with CM500S (t = 1.0 mm) as an IR cut filter and image at F8. The luminous intensity to the sensor receiving surface at this point is defined as the standard sensitivity testing luminous intensity.
[b]User measured data.

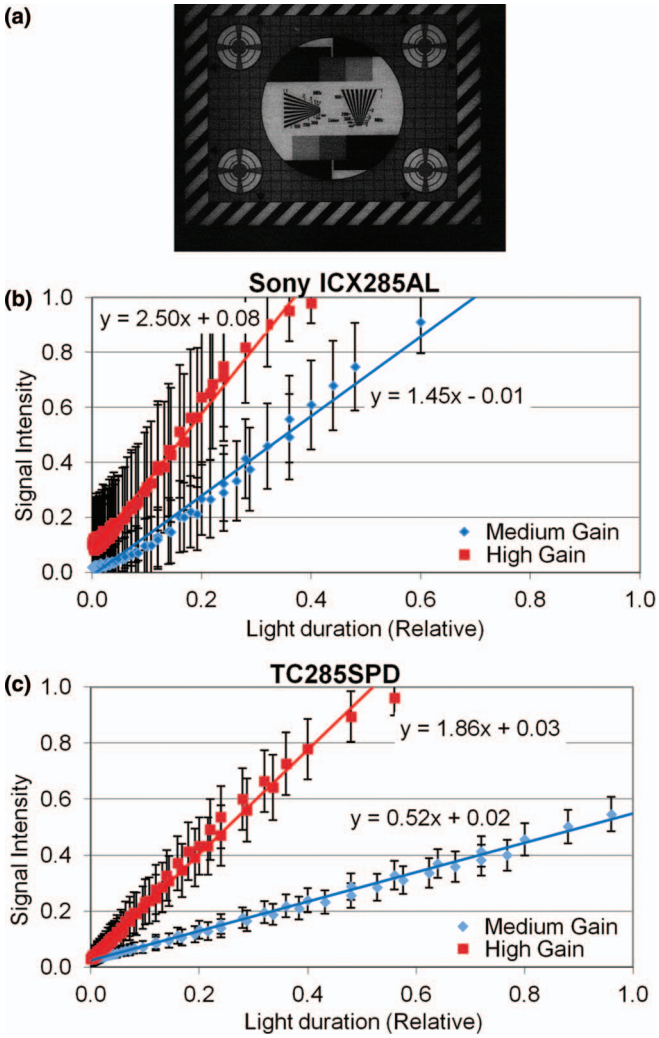

FIG. 8. Testing procedure for relative sensitivity of candidate CCDs. (a) A TV chart was imaged with a single light pulse at various durations with all candidate cameras. (b) and (c) Linear fits of normalized image brightness in selected region of interest vs. light level for various gain/contrast settings. (b) Data from the Lumenera camera ultimately chosen for our system. (c) Data from the TI EMCCD chip contained in the Hamamatsu C9100-02 camera.

B. Sensitivity

The relative normalized slopes for each camera using the best performance value of ICX055AL as a reference are listed in Table I. This parameter is a range rather than a single number because the values varied with the exact gain, contrast, and brightness settings used for a given set of test conditions. All three candidate cameras were more sensitive compared with the ICX055AL, by more than 17 times (based on S_0). From the values of S_0 alone, the ICX429AL was more sensitive than the other candidates. However, this is due to the much larger area of the photo-cell. It was found that the ICX285AL was more sensitive if the slope was further normalized by the cell area (based on S_1). For single shot applications, the 2:1 interlace of the ICX429AL effectively reduced the vertical resolution by a factor of 2 (only every other line is available). Therefore, the ICX429AL was removed from further consideration.

The choice between the ICX285ALL and the TC285SPD was not obvious based on normalized slope alone. However, we noticed that the TC285SPD produced better quality images at low lighting conditions. Therefore, L_{02} as defined above and derived from the data in Fig. 8 was compared between these cameras. It was found that the L_{02} value for the ICX285AL was 2.6 times of that of TC285SPD. This indicates that the TC285SPD is 2.6 times more sensitive at forming usable images at extremely low lighting conditions. This can be explained by the extensive cooling used in TC285SPD that reduced dark current. However, ultimately, the ICX285AL was chosen over the TC285SPD for our system due to cost and size considerations.

C. Resolution

The resolution of our integrated system under high speed conditions was tested with a high resolution target (1951 USAF Glass Slide Resolution Targets, Edmund Optics Inc., Barrington, NJ). Figure 9(a) shows the image of the target with a 100× objective lens at 5 Mfps. The finest element on this target is shown in the highlighted area, with a specified resolution of 645.08 lp/mm. Horizontal and vertical

TABLE II. Comparison of main characteristics of UPMC Cam to other high speed camera types.

	Rotating mirror	Electronic	Brandaris	UPMC Cam
Media	Film	Intensified CCD	CCD	CCD
Frame rate (Mfps)	25	200	25	25
Number of frames	130	8	128	128
No. of runs	1	2	6[a]	2
Turnover time (s)	1800	60	1	1
Total number of frames	130	16	768	256
Minimum time between runs	60 s	4 μs	20 ms	50 μs
Pixel count (H × V)			500 × 292	920 × 616
Image size (pixels)			146 k	567 k
Pixel size (μm, H × V)			9.8 × 12.6	6.45 × 6.45
Bit depth (bits)			8	12

[a]The Brandaris has been updated to include region of interest and segment modes. See Ref. 25.

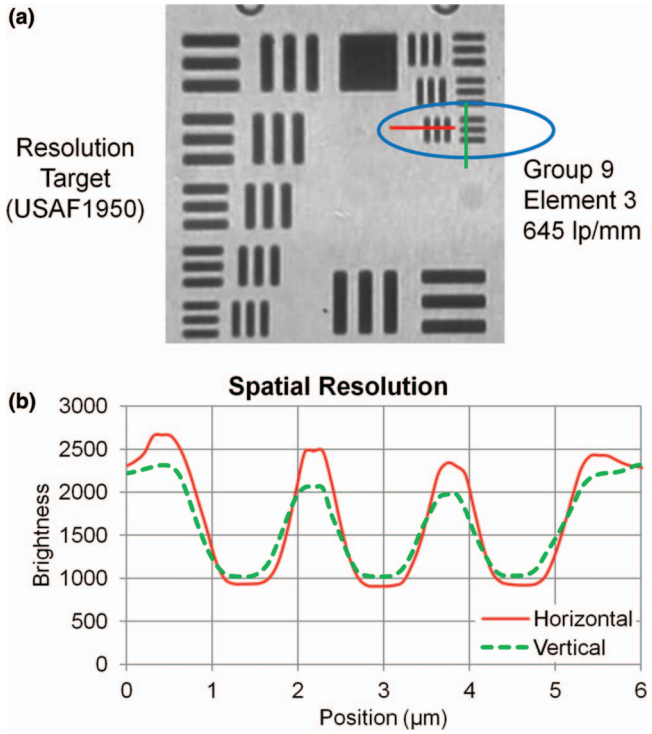

FIG. 9. Spatial resolution of the imaging system. (a) High resolution target under the microscope. (b) Horizontal and vertical profiles of this area demonstrate the resolving power of the system.

profiles of this area are shown in Fig. 9(b). The contrast transfer function was derived as normalized contrast $C = (B_{max} - B_{min})/(B_{max} + B_{min})$ in the profile where B_{min} and B_{max} are the minimum and maximum values, for each of the elements on the test target. The modulation transfer functions derived from contrast transfer function vs. specified resolution demonstrate resolving power of our system at 0.5 μm, nearing the diffraction limit of the microscope system.

D. Example images

1. Feasibility of high speed multi-frame fluorescence imaging

Figure 10 shows selected frames from fluorescence movies of reference beads with mean size of 1, 2, and 4 μm (Bangs Lab, Fishers, IN) at 25 Mfps. In this figure, only 16% of the total number of pixels are shown. Note our ability to visualize 1 μm spheres. These data suggest the potential for *in vivo* intravital microscopy of vibrating fluorescent MBs in the microcirculation.

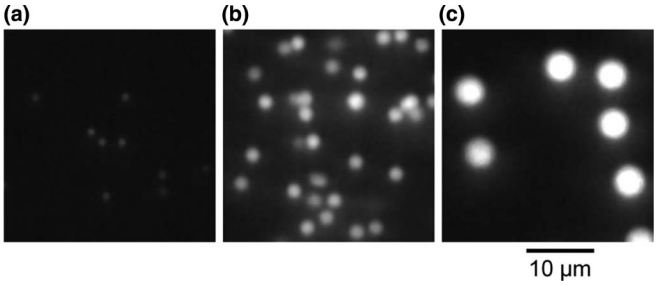

FIG. 10. Selected frames from fluorescence movies of reference beads at 25 Mfps. (a) 1.01 μm beads; (b) 1.90 μm beads; (c) 4.16 μm.

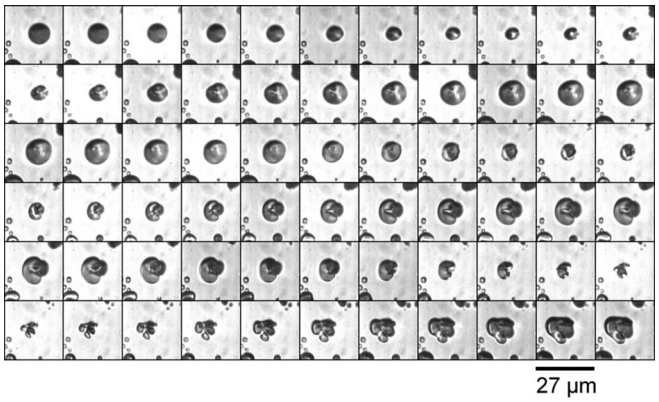

FIG. 11. A bright field movie of lipid MBs under US excitation (f = 2.25 MHz, P_a = 1.0 MPa), demonstrating US-induced MB vibration and breaking. Imaging is at 25 Mfps and playback is at 16 fps. Cropped to 256 × 256 pixels. Frame size is 27 μm × 27 μm (enhanced online). [URL: http://dx.doi.org/10.1063/1.4809168.1]

2. Brightfield imaging of dynamic behavior of MB

Figure 11 shows a bright field movie at 25 Mfps of a lipid MB interaction with US energy (f = 2.25 MHz, P_a = 1.0 MPa), showing MB shape deformation, breaking, and possible jet formation.

3. Comparison between bright field and fluorescence images of MB dynamic behavior

We have also performed high speed bright field (Fig. 12) and fluorescence imaging (Fig. 13) of PDLLA polymer MBs labeled with R-PE under identical US excitation conditions (f = 1 MHz, P_a = 2.0 MPa) at 25 Mfps. Fluorescence imaging can help determine the fate of the MB shell. In this study, the bright field movie shows violent oscillations of the MBs.

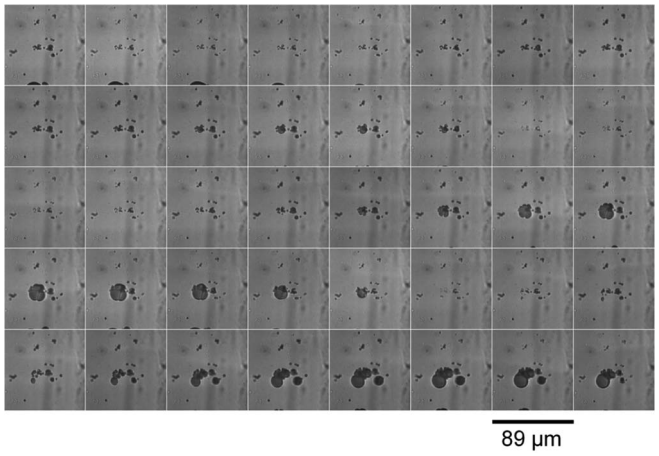

FIG. 12. A bright field movie of polymer MBs under US excitation (f = 1 MHz, P_a = 2.0 MPa) demonstrating violent MB oscillations. Imaging is at 25 Mfps and playback is at 16 fps. Cropped to 512 × 512 pixels. Frame size is 89 μm × 89 μm (enhanced online). [URL: http://dx.doi.org/10.1063/1.4809168.2]

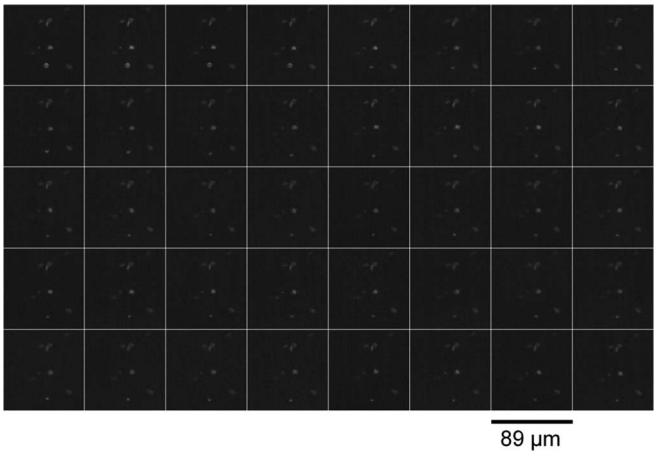

FIG. 13. A fluorescence movie of fluorescently labeled polymer MBs under US excitation ($f = 1$ MHz, $P_a = 2.0$ MPa) showing lower amplitude oscillations of the fluorescent MB shell, despite violent oscillations of the gas during bright field imaging (Fig. 12). Imaging is at 25 Mfps and playback is at 16 fps. Cropped to 512 × 512 pixels. Frame size is 89 μm × 89 μm (enhanced online). [URL: http://dx.doi.org/10.1063/1.4809168.3]

The fluorescence movie (5 W laser pulse used) shows smaller amplitude oscillations of the MB shell material, suggesting that violent oscillations seen on bright field imaging are from the gas that has escaped from the MB shell. This observation may have implications for US mediated therapy such as drug and gene delivery.

V. CONCLUSION AND DISCUSSION

We have developed a high speed imaging system capable of 25 Mfps for both bright field and fluorescence imaging. The capability for high speed imaging of both fluorescent micrometer-sized objects at rates up to 25 Mfps (Fig. 10) as well as oscillating fluorescent MBs (Fig. 13) is unique to our system and incremental to the capabilities of existing high speed cameras (17). To our knowledge, our camera system is the only system available in the world that allows microscopic fluorescence recordings for long record length at multi-million frame rates.

To achieve microscopic fluorescence imaging at high speed we employed several strategies: First, we performed rigorous systematic testing of several commercially available CCD cameras to identify the most sensitive commercially available CCD with sufficient resolution for our application. While the EMCCD proved to be the most sensitive camera system tested, the incremental sensitivity was felt not to outweigh the order of magnitude increase in cost. Second, we manipulated lighting conditions to maximize photon emission from a given fluorophore, which requires higher energy and specific wavelength excitation not provided by a traditional flash lamp. To achieve this, a laser system was custom designed to deliver a high energy light pulse (5 W at 488 nm) that could be sustained over the duration of light exposure necessary for acquiring 128 images at 0.64-25 Mfps. A disadvantage of this approach is that it limits our use of fluorophores to the ones that have excitation spectra with peaks near 488 nm. It would be necessary to change to a different laser head for other types of fluorophores. However, the camera system would work with similar sensitivity in other commonly used wavelengths such as 532 nm. A custom 5-axis fiber alignment system was also deployed for the effective delivery of the pulsed laser energy through the fluorescence light path. A third strategy is to identify or develop fluorophores for the MB that has higher total emission cross section such that more photons are generated for a given incident light configuration. Simply adding more fluorophore to the MB formulation is not an optimal strategy for increasing fluorescence, as loading large amounts of fluorophore onto the MB shell could alter the acoustic behaviors. The resulting system has enabled, for the first time, the acquisition of a fluorescence movie of micrometer-size objects at 25 Mfps for 128 frames.

The fluorescence images of the MBs at very high speed produced from our system are far from perfect. High CCD gain was required, so images are relatively noisy. It is difficult to observe all the borders of the MB. A more costly EMCCD design could have provided more sensitivity with sufficient spatial resolution for our purpose. This potential improvement might be useful for intravital microscopy studies as photon loss due to tissue attenuation may make it more difficult for high speed fluorescence imaging.

The spatial resolution of our system is sufficient for MB observations. Importantly, advanced timing control of the system will allow observation of interaction between US, MB, and biological cells at different points during a given pulse sequence. In this regard, our unique ability to set an advance trigger to allow US delivery to begin up to 125 ms (depending on the frame rate) prior to image acquisition is particularly advantageous. This critical feature allows us to visualize MB events at various time points of relatively long acoustic tone bursts, which is a crucial capability as the therapeutic efficacy of long pulses for therapeutic applications has become evident.[12,31]

In conclusion, our imaging system is capable of both bright field and fluorescent *in vitro* imaging of MBs at high speed. Its high speed fluorescence imaging capabilities confers the potential for *in vivo* (fluorescent) high speed observations during intravital microscopy. Advanced timing control allows unique options for studying MB behaviors, heretofore never seen, under the influence of new US regimes involving long tone bursts. The optical data from this system could increase our understanding of the mechanisms of US-MB bioeffects and *in vivo* MB behaviors in response to US, ultimately facilitating the development of US-MB mediated therapy and molecular imaging for cardiac and other diseases.

ACKNOWLEDGMENTS

This study was financially supported by a grant from the University of Pittsburgh Medical Center. The authors would like to thank Sid Nebeker, Alex Wenzel, Vance Parker, Joe Ouellette, Bill Larkin, Steve Holtman, Michael Woznokoviak, and Susan Palmer from Cordin Company for their unswerving commitment to this project and creative collaboration in the development of this system. We would also like to thank Dr. Erik Gelderbloom (University of Twente) for his technical support during CCD testing.

[1]B. Gabriel and J. Teissie, Biophys. J. **76**(4), 2158 (1999).
[2]D. May, J. Allen, J. Gut, and K. Ferrara, *IEEE Ultrasonics Symposium* (IEEE, New York, 2001), p. 1385.
[3]P. Marmottant and S. Hilgenfeldt, Nature (London) **423**(6936), 153 (2003).
[4]N. de Jong, P. J. A. Frinking, A. Bouakaz, M. Goorden, T. Schourmans, J. P. Xu, and F. Mastik, Ultrasound Med. Biol. **26**(3), 487 (2000).
[5]J. E. Chomas, P. A. Dayton, D. May, J. Allen, A. Klibanov, and K. Ferrara, Appl. Phys. Lett. **77**(7), 1056 (2000).
[6]M. Postema, A. Bouakaz, C. T. Chin, and N. de Jong, IEEE Trans. Ultrason. Ferroelectr. Freq. Control **50**(5), 523 (2003).
[7]F. S. Villanueva, JACC: Cardiovasc. Imaging **3**(9), 944 (2010).
[8]F. S. Villanueva, E. Lu, S. Bowry, S. Kilic, E. Tom, J. Wang, J. Gretton, J. J. Pacella, and W. R. Wagner, Circulation **115**(3), 345 (2007).
[9]A. R. Carson, C. F. McTiernan, L. Lavery, M. Grata, X. Leng, J. Wang, X. Chen, and F. S. Villanueva, Cancer Res. **72**(23), 6191 (2012).
[10]M. Kaya, C. Toma, J. Wang, M. Grata, H. Fu, F. S. Villanueva, and X. Chen, Ultrasound Med. Biol. **38**(11), 1989 (2012).
[11]J. T. Sutton, N. M. Ivancevich, S. R. Perrin, Jr., D. C. Vela, and C. K. Holland, Ultrasound Med. Biol. **39**(5), 813 (2013).
[12]J. E. Leeman, J. S. Kim, F. T. H. Yu, X. Chen, K. Kim, J. Wang, X. Chen, F. S. Villanueva, and J. J. Pacella, Ultrasound Med. Biol. **38**(9), 1589 (2012).
[13]T. G. Etoh, D. Poggemann, G. Kreider, H. Mutoh, A. J. P. Theuwissen, A. Ruckelshausen, Y. Kondo, H. Maruno, K. Takubo, H. Soya, K. Takehara, T. Okinaka, and Y. Takano, IEEE Trans. Electron Devices **50**(1), 144 (2003).
[14]T. G. Etoh, D. H. Nguyen, S. V. T. Dao, C. L. Vo, M. Tanaka, K. Takehara, T. Okinaka, H. van Kuijk, W. Klaassens, J. Bosiers, M. Lesser, D. Ouellette, H. Maruyama, T. Hayashida, and T. Arai, in *Proceedings of the IEEE International Solid-State Circuits Conference Digest of Technical Papers (ISSCC)* (IEEE, San Francisco, 2011), p. 406.
[15]B. Brixner, in *Proceedings of the 20th International Congress on High Speed Photography and Photonics*, edited by J. M. Dewey and R. G. Racca (SPIE, Bellingham, 1992), p. 52.
[16]C. T. Chin, C. Lancee, J. Borsboom, F. Mastik, M. E. Frijlink, N. de Jong, M. Versluis, and D. Lohse, Rev. Sci. Instrum. **74**(12), 5026 (2003).
[17]M. Postema, A. van Wamel, C. T. Lancée, and N. de Jong, Ultrasound Med. Biol. **30**(6), 827 (2004).
[18]A. van Wamel, A. Bouakaz, M. Versluis, and N. de Jong, Ultrasound Med. Biol. **30**(9), 1255 (2004).
[19]A. Bouakaz, M. Versluis, and N. de Jong, Ultrasound Med. Biol. **31**(3), 391 (2005).
[20]A. van Wamel, K. Kooiman, M. Harteveld, M. Emmer, F. J. ten Cate, M. Versluis, and N. de Jong, J. Controlled Release **112**(2), 149 (2006).
[21]S. M. van der Meer, B. Dollet, M. M. Voormolen, C. T. Chin, A. Bouakaz, N. de Jong, M. Versluis, and D. Lohse, J. Acoust. Soc. Am. **121**(1), 648 (2007).
[22]M. Overvelde, V. Garbin, J. Sijl, B. Dollet, N. de Jong, D. Lohse, and M. Versluis, Ultrasound Med. Biol. **36**(12), 2080 (2010).
[23]J. Sijl, H. J. Vos, T. Rozendal, N. de Jong, D. Lohse, and M. Versluis, J. Acoust. Soc. Am. **130**(5), 3271 (2011).
[24]M. Versluis, D. E. Goertz, P. Palanchon, I. L. Heitman, S. M. van der Meer, B. Dollet, N. de Jong, and D. Lohse, Phys. Rev. E **82**(2), 026321 (2010).
[25]E. C. Gelderblom, H. J. Vos, F. Mastik, T. Faez, Y. Luan, T. J. A. Kokhuis, A. F. W. van der Steen, D. Lohse, N. de Jong, and M. Versluis, Rev. Sci. Instrum. **83**(12), 103706 (2012).
[26]V. Parker and C. Roberts, "Rotating mirror and drum cameras," in *High Speed Photography and Photonics*, edited by S. F. Ray (SPIE Press, Bellingham, 1997), p. 167.
[27]C. D. Miller, J. SMPE **53**(5), 479 (1949).
[28]E. A. Igel and M. Kristiansen, *Rotating Mirror Streak and Framing Cameras* (SPIE Optical Engineering Press, Bellingham, 1997), p. 59.
[29]S. Ottoboni, R. E. Short, M. B. Kerby, E. G. Tickner, E. Steadman, and T. B. Ottoboni, Contrast Media Mol. Imaging **1**(6), 279 (2006).
[30]G. E. Weller, F. S. Villanueva, E. M. Tom, and W. R. Wagner, Biotechnol. Bioeng. **92**(6), 780 (2005).
[31]X. Chen, J. E. Leeman, J. Wang, J. J. Pacella, and F. S. Villanueva, "New insights into mechanisms of sonothrombolysis using ultra high speed imaging," Ultrasound Med. Biol. (submitted).